

111

Field Measurements of Flow in Lateral Separation Eddies on the Colorado River in Grand Canyon

Richard R. McDonald and Jonathan M. Nelson

USGS, Denver Federal Center, Lakewood, CO. 80225

Abstract

Lateral recirculation zones are the principal zone of sediment storage in canyon rivers dominated by debris flow fans such as the Colorado River in Grand Canyon. Sediment deposits within these zones have been identified as important environmental and recreational resources. A physical understanding of the transfer of sediment from the main channel into the lateral recirculation zone is crucial to developing a predictive flow and sediment-transport model to aid management decisions related to these resources.

We measured the vertical structure of flow along the reattachment streamline in three lateral recirculation zones in order to provide data for assessing sediment exchange mechanisms and to provide data for testing existing numerical models. Measurements were made using a newly developed current meter profiling system consisting of a weighted, free-rotating 2 m rod equipped with four current meter triplets and a large fin to keep the current meters oriented into the mean flow. Each current meter triplet measures three components of flow at turbulence-resolving frequencies. Substantial contamination of the data resulting from suspended organic matter clogging the current meters prohibits the calculation of turbulence quantities, but careful editing of the data provides good estimates of mean flow quantities. These estimates along with bathymetric measurements are used to describe the general circulation pattern in the eddies and to describe the temporal and spatial variability. The measurements are contrasted with more detailed measurements in simple flat-bedded lateral separation eddies. The results show both similarities and significant differences between the sediment-filled eddies measured in the field and the simpler, flat-bedded, laboratory cases. Potential mechanisms for producing the observed differences appear to be related to steep lateral slopes found along the riverward margin of the natural separation eddies. A more complete understanding of the evolution of the flow field during the transformation of initially empty eddies into well-

developed, topographically complex eddies, and the effect of the evolving flow field on sediment trapping, requires further detailed mapping of the flow field and consideration of the local fluctuations about the mean flow field.

Introduction

Purpose

Lateral separation eddies occur in rivers or streams where the principal downstream flow separates from the river bank in regions of relatively high planform curvature (e.g., meander bends with small radii of curvature) or in reaches where there is an abrupt expansion in channel width (e.g., downstream of bank irregularities such as debris fans produced by tributary sediment inputs). In this paper, lateral separation eddies of the second type are considered, although many of the observations and conclusions presented herein are general in nature. In response to the increase in channel width, flow separates from the bank of the river near the apex of the expansion and reattaches some distance downstream, forming a zone of relatively weak recirculating flow (Figure 1).

Lateral separation zones are efficient traps and storage zones of sediment and organic debris, as evidenced by the deposits commonly found within them. These deposits provide substrate for riparian habitat, and the morphology of the deposits creates nearly stagnant back-water areas that have been identified as important habitat for endangered fish. In regulated rivers, the stability of these deposits to erosion and deposition is sensitive to the imposed flow discharge history (Schmidt and Rubin, 1995). As a result of the link between riverine ecology and the morphology of lateral separation zones, and the recreational importance of lateral separation zone deposits (Kearsley et al., 1994)

developing a mechanistic understanding of the roles of various discharge regimes in the maintenance of lateral separation zones and their deposits is a critical part of riverine management.

The purpose of this paper is to report observations of flow patterns in lateral separation zones, specifically those formed in the lee of debris fan constrictions in the Colorado River in the Grand Canyon, and to use those measurements to gain further insight into the nature of flow and sediment transport mechanics operative in lateral recirculation zones. In addition, the detailed observations of flow in a natural eddy reported herein provide an opportunity to test the applicability of existing numerical models for flow in lateral recirculation zones by assessing the importance of various physical mechanisms that may or may not be included in existing modeling approaches. The latter, discussed near the end of this paper, is a crucial step in verification of predictive models of both flow and sediment transport in lateral separation zones that may be used as tools for the management of regulated rivers.

Previous work

The location, general flow pattern and sedimentary characteristics of lateral recirculation zones and their deposits in the Colorado River in Grand Canyon have been described in general by Howard and Dolan (1981) and more specifically by Schmidt and Graf (1990), Schmidt (1990), and Rubin et al. (1990). Schmidt (1990) found that the recirculation zone generally consists of a large primary eddy and possibly one or more smaller secondary eddies. The instantaneous length of the recirculation zone (the distance from the separation point to the reattachment point) fluctuates in the streamwise direction

about some mean reattachment point (Rubin et al., 1990; Rubin and McDonald, 1995). The mean reattachment length generally increases as the discharge increases but may be complicated by overtopping of the debris fan (Schmidt and Graf, 1990) or downstream irregularities in the channel geometry (Schmidt et al., 1993). Within these recirculation zones Schmidt (1990) defined two principal types of deposits reflecting the hydraulic characteristics in which each is found; separation bars and reattachment bars (Figure 1). Reattachment bars form along the reattachment zone and extend into the primary eddy and separation bars mantle the debris fan or other constriction at the upstream end of the recirculation zone near the separation point. Rubin et al. (1990) looked at the internal structure of a reattachment bar to gain insight into the flow processes and the evolution of the bar. Their observations of the migration patterns of bars and ripples were consistent with the recirculating pattern of flow within the eddies and the large upstream-downstream fluctuations of flow at the reattachment point.

Laboratory measurements of flow in a simple rectilinear expansion show that the effective sediment-trapping mechanism in lateral recirculation zones is associated with advective transport of sediment into the eddy by secondary flow across the reattachment streamline (Nelson, 1991; Nelson et al., 1995). This secondary flow is driven by the interaction of vortices generated in the free shear layer along the reattachment streamline with the vertical shear in the streamwise flow. This interaction results in downstream tilting of the vortices axis of rotation and generates mean flow into the eddy near the bed and out of the eddy near the surface relative to the reattachment streamline (which, unlike the case of a purely two-dimensional separation zone, is a streamline only in a vertically

averaged sense; see Nelson and McDonald, 1995) joining the separation and reattachment points. The correlation of mean flow into the eddy near the bed with relatively high sediment concentrations near the bed produces an effective method for transporting sediment from the channel into the eddy.

In addition to the role of secondary flows, sediment trapping in eddies is enhanced as a result of the relatively low-frequency unsteadiness generated by the flow separation and reattachment process. The shedding and downstream advection of vortices along the reattachment streamline affect both the magnitude and frequency structure of flow variation in lateral recirculation zones under both field and laboratory conditions (Rubin and McDonald, 1995). Flume experiments show large pulsations in the flow created by the passage of vortices along the reattachment streamline. The spatial variability of the frequency structure of flow associated with the production and advection of vortices from near the separation point is complicated, shifting from relatively high-frequency variability near the separation point to low-frequency variability near the reattachment point (Nelson et al., 1995). While mean flow fields characterize the general rotary pattern of flow in lateral recirculation zones and steady-state computational models that predict mean flow fields to drive sediment transport appear to sufficiently simulate the general evolution of reattachment bars as recorded in flume experiments where sediment moves only as bedload (Nelson et al. 1994), it is clear that unsteadiness associated with flow separation and the geometry of the lateral separation zone plays an important, but poorly understood role in the sediment-transport dynamics.

Study area

The geology and geomorphology (Leopold, 1964; Howard and Dolan, 1981) and the hydraulic setting and recent flow history (Schmidt and Graf, 1990; Kieffer, 1985) of the Colorado River in Grand Canyon have been described extensively. Our study measured flow in three lateral separation eddies (Figure 2) in the Colorado River, located at river mile 44.2 (Eminence Break Camp, site 1), river mile 64.7 (Carbon Creek, site 2) and river mile 122.0 (One Hundred Twenty Two Mile Creek Camp, site 3; names and mileage as in Schmidt and Graf, 1990, appendix A). Each site is located downstream of a large channel constriction formed by a debris fan. The morphology of the reaches at sites 1 and 2 are similar; each is relatively straight and unconstrained, meaning that there are no lateral flow constrictions downstream of the lateral recirculation zone. However, within the lateral recirculation zone, site 1 is relatively depleted of sediment compared to site 2. In contrast, site 3 is located in a sharp meander formed by closely spaced debris fans on opposing sides of the river. During our study flow releases from Glen Canyon dam fluctuated between steady high and low discharge. Flow measurements were made during steady high flow ($\approx 425 \text{ m}^3/\text{s}$) at the first two sites and both high and low flow ($226 \text{ m}^3/\text{s}$) at site 3 (Figure 3).

Methods

Velocity measurements

In order to measure vertical profiles of velocity in the Colorado River in Grand Canyon, we developed a current meter profiling system (Figure 4). The profiling system consists of four measuring points spaced on a 2 m free-rotating, stainless-steel weighted

rod equipped with a large fin to keep the current meters oriented into the mean flow. Each measuring point comprises 3 small impeller driven current meters, 10 cm apart horizontally, with the axis of each current meter oriented orthogonally to the others, allowing the measurement of three orthogonal components of velocity. To avoid potential problems with threshold velocities (about 1 cm/s for these devices), the orthogonal current meter orientations were chosen such that each current meter had a significant component of the principal flow direction (as determined by the fin) along its axis. The current meter rotors are 3.5 cm in diameter and are held in a 1.6 cm long, 4.2 cm diameter duct. This design has been shown by others (Smith, 1978) and independently by ourselves to have a directional response within 90% of an ideal cosine response for angles up to 70 degrees between the incoming flow vector and the current meter axis (McDonald and Nelson, USGS Open-File Report, in prep 1995) A small magnet imbedded in one of the four rotors generates a pulse-type signal as it rotates past a Hall effect sensor embedded in the support rod; as the Hall effect sensor is sensitive to the magnetic polarity, this pulse provides information on both the rotation speed and direction of rotation of the impeller.

The signals from all twelve current meters of the profiling array were sent via cable to a watertight signal junction box attached to the profiler. A single cable from the junction box connects the profiling system to a PC-laptop computer on board the support boat. The junction box contains an electronic interface which sequentially scans the signal from each of the 12 current meters every 320 microseconds and evaluates the current state of each current meter. Each time a change in the current meter state is recorded, a 2-byte word is sent to the computer containing the rotation direction of the current meter

impeller, the current meter address, and the time since the last rotation. The junction box also contains a gimbaled compass capable of recording changes in the heading at approximately 16 Hz. The complete signal then contains the velocity of each current meter and the orientation of the profiler.

The current meter profiler was deployed from a modified USGS bridge crane mounted to the front of a 20' catamaran raft. We used a three point anchoring scheme to keep the boat in a stationary position. We were able to position the profiling system generally where desired but fine adjustments on the order of 5 - 10 meters were difficult, especially when trying to position directly adjacent to the reattachment streamline. The measuring process consisted of first positioning the boat as close as possible to the desired measurement location, which was generally either the eddy side of the reattachment stream line or in the return channel where upstream flow was relatively strong. At each measuring station, we lowered the profiler to just above the river bed and collected data for approximately 3-5 min., depending on the flow velocity and/or the degree of contamination by suspended organic matter. If the depth was greater than the column measured by the profiler, we raised the profiler to a depth just above the last highest measuring point or overlapped the last position as needed and the process was repeated.

Ultimately, the desired flow information consists of the mean vertically averaged velocity vector at each measuring station and the variation of the down-stream and cross-stream components of flow about the mean vector. This process is achieved by first interpolating the the velocities to an evenly spaced data time series. We do this in the simplest way by choosing a sampling frequency close to, but higher than, the greatest

frequency of the current meter rotation. We arbitrarily chose the sampling frequency the compass. At each sampling time for the interpolated series, the velocity is set equal to the most recently acquired velocity in the full time series; if the velocity has changed, then the velocity is updated, if it hasn't, the velocity is simply chosen to be the last recorded value. Second, the velocities are rotated from the collecting frame of reference to the desired u , v , and w frame of reference where u is oriented along the mean vertically averaged vector, v is oriented in the cross-stream direction, orthogonal to u , and w is vertical and perpendicular to the u - v plane. To do this, the data are first rotated into the reference frame of the fin whose heading at each time step is known. At each measuring position on a vertical profile, a mean northing and easting map component of flow can be calculated from the velocity components relative to the fin heading and averaged vertically to get the mean vertically averaged velocity vector. Once the mean vector is found the northing and easting velocity time series are rotated into the right-hand coordinate system defined by the mean vector to obtain a time series of u , v , and w velocity components.

The primary problem encountered in the data collection was clogging of the current meters due to suspended organic matter. As shown in (Figure 5), some measuring points were completely undisturbed while others were contaminated soon after collection began. As a result, approximately 30% of the data were discarded and, in measuring locations where more than one profiling position was measured the data were only rarely of the quality necessary to obtain a good velocity profile. In addition, estimates of turbulence quantities, especially higher moments of velocity distributions, were not accurate, as even very minor or brief fouling can produce significant error. In general, careful editing of the

velocity data allowed reasonable estimates of the mean vertically averaged velocity vectors, some profile information, and piecewise estimates of turbulence intensities. For each measuring point analyzed, the longest undisturbed piece of the velocity time series was employed. If one of the three current meters was completely contaminated then two were used assuming the mean vertical velocity was zero to do the necessary rotations.

Bathymetry and Topography

For each eddy studied, topographic maps were constructed that included both bathymetry and topography. The topographic data consisted of three data sets; above water (141 m³/s) digital topography provided by Grand Canyon Environmental Studies, surveyed topography at and near the edge of water (ground surface approximately 2 m above water surface and 1 m below water surface), and bathymetry obtained with echo soundings. The last two items were collected synchronously with our velocity data. All three data sets were merged into a single data set. The ground surface surveyed topography was crucial in accounting for changes in the eddy bar topography over the time between the collection of the above and below water topography. The entire data set consists of randomly spaced elevation data. We used a gridding algorithm provided by General Mapping Tools (GMT) (Smith and Wessel, 1990) to construct an evenly spaced grid of elevation data from which topographic maps of each eddy were created. Visual comparison between the contours created by the GMT contouring routine with the above water digital data and the correlation of the depths at each measuring point with our

measured depths at those points provide reasonable confidence in the topographic form of the eddies as depicted by the contour maps.

Results

Eddy topography

All three eddies have remarkably similar characteristics in terms of both the geometry of the deposit within the eddy and the geometry of the adjacent main channel. A pronounced increase in the bed slope of the main channel begins near the apex of the channel expansion. This deepening continues well beyond the downstream end of the debris fan, forming a deep pool adjacent to and continuing along the length of the eddy. Near the downstream limit of the eddy deposit, the flow in the main channel begins to shoal in the streamwise direction. Previous flume studies (Schmidt et al. 1993; Nelson, 1991; and Nelson et al., 1995) and modeling studies (Miller, 1994; Nelson et al., 1994) of flow and sediment transport in lateral separation eddies have investigated eddy dynamics in the absence of these deep confined pools created by a rapid increase in the thalweg slope. In light of the sensitivity of eddy geometry to main channel morphology demonstrated by Nelson et al. (1994), it appears that this feature may play an important role in determining the maximum streamwise extent of the eddy.

The deposits within the eddy at the time of this study were primarily reattachment bars. Geomorphically, they take the form of an active reattachment bar inset into an older bar formed during higher flows. The reattachment bar appears as a platform dipping gently upstream and towards the main channel where the slopes become quite steep,

approaching the angle of repose (Figure 6). The deposit is bounded on one side by the main channel and on the other by the return channel. The peak elevation of the reattachment bars are located near the greatest possible historical downstream location of the reattachment. The return channel may be broken into two sections: 1) along the shoreward margin of the active eddy and 2) downstream of the active eddy. The latter section of the return channel is intermittent and presumably reflects activity at much higher flows. The active return channel generally deepens upstream with a sharp increase in slope near the exit to the main channel.

Flow Fields

At all three study sites, we determined the vertically averaged velocity vectors at each measuring position and the mean downstream and cross-stream velocity profiles in the reference frame determined by the vertically averaged velocity. As noted above, measurement efforts focused along the reattachment streamline and in the return channel. Figure 7 shows results from site 1. The mean flow shows a rotary flow pattern with return flow near the channel bank, as expected. The flow accelerates as it exits the eddy in response to the focusing of flow in the return channel. The strong correlation of the mean velocity direction with the contours of the bed at measuring positions 9 - 13 near the reattachment point suggest the flow is steered topographically in this region. Upstream flow at measuring position 1 suggests the presence of a small secondary eddy, in agreement with the observations of a similar eddy found at somewhat higher flow by Schmidt and Graf (1990).

As noted above, the presence of secondary flows along the reattachment streamline has been observed in simple eddies created in the laboratory and also predicted computationally for those situations. However, this phenomenon has been studied almost exclusively for the case of initially empty (i.e., flat-bedded) eddies. It seems likely that the development of the eddy deposit and variations in the main channel bathymetry may have some role in the modification of effect, as supported by our more recent computational results (Nelson et al. 1994). Using the field data, it is possible to evaluate the presence or absence of secondary flow along the reattachment streamline. The current meter contamination and limited number of data points in the vertical dictate that caution be used in interpreting details of the mean velocity profiles. However, consistency between points 2 and 3 (see Figure 7 for location), located near the separation point in a region with relatively shallow (approximately 7° , Figure 6) cross-channel slopes, suggests there is weak inward flow near the bed (the mean flow depth is 325 cm and the average of points 2 and 3 are $u \approx 25$ cm/s and $v \approx 1.3$ cm/s at ≈ 81 cm above the bed) and weak outward flow near the surface (the average of points 2 and 3 are $u \approx 14.6$ cm/s and $v \approx -2.8$ cm/s at 281 cm above the bed), consistent with results from the flat-bedded case.

In contrast, at both positions 7 and 8, located in a region of relatively steep cross-channel slopes (approaching the angle of repose, Figure 6), the rose diagrams in Figure 7 show a bimodal distribution of flow direction at depth and a component of this distribution directed out of the eddy into the main channel at depth. In addition, at both these measuring positions the heading time series nearest the surface has less variability than

those at depth. The flow turns rapidly near position 9 and is directed nearly straight into the eddy with more upstream flow near the bed than at the surface.

All points along the reattachment streamline (2 - 8) show maximum velocities at depth indicating the presence of a high velocity core at depth in the main channel. In general, the turbulence intensities are 50% - 100% of the mean flow along the reattachment line and 5% - 24% of the mean velocity in the return channel.

Similar results are found at sites 2 and 3, but we focus on site 3, because this site included measurements at both high and low discharges. General observations at site 3 (Figure 8) include a rotary pattern of flow within the eddy at both high and low discharge with greater flow velocities during high discharge, as expected. At those measuring points near the downstream, end of the eddy in the main channel (pts 15 & 16 at low discharge and 23-26 at high discharge), the variation in flow velocities is less than at those points in the eddy or on the margin of the eddy. There is a much greater variation in flow direction for most points at low discharge, however it is unclear whether this is a function of the discharge or a function of the measuring locations which are generally nearer to the break in slope of the eddy deposit at low discharge compared to the points at high discharge, which are closer to the shore. Looking more specifically at the variations in the flow field at site 3, and focusing on those points near the separation point (1-6 at low flow and 7 - 9 at high flow, see Figure 8) we find the flow is directed upstream, in contrast to those points (2-4) nearest the separation point at site 1 (Figure 7). Low flow measuring points 5 and 6 (Figure 8), located in a deep embayment in the eddy deposit that appears to have a significant influence on the flow. The variations in heading displayed in the rose diagrams

at measuring point 6 show large variations in flow direction with depth, including upstream flow near the surface, inward flow at mid-depth (time series of heading variations at this locations shows the current meter spun around twice), and outward flow at the deepest location.

Discussion

Flow Variability

Flume studies of lateral separation eddies have quantified some aspects of the spatially complex nature of the frequency and magnitude of variation about the mean flow field (Schmidt et al. 1992; Rubin and McDonald 1995 and Nelson et al., 1995). Many more detailed flume studies have looked at the frequency structure of the flow field behind a backward or negative step (see, Eaton and Johnson, 1980; Driver, 1987; Simpson, 1989; and Nelson et al., 1995). In general, the latter studies show a downstream evolution in the large scale vortex structures associated with vortex shedding from relatively small amplitude-high frequency structures to relatively large amplitude-low frequency structures. In the lateral separation case, the manner in which these variations about the mean flow field affect the sediment trapping rate or the development of the reattachment and separation bars is poorly understood. However, in light of the non-linear relationship between flow and sediment transport, it is clear that these variations play a significant role and, as a result, there is clearly a need to better understand the spatial pattern in frequency and magnitude of flow variation in lateral separation eddies.

To better understand the spatial variability of the frequency and magnitude structure of the flow variation, a more complete mapping of the flow field than we were able to do would be desirable. Nevertheless, we can gain some insight into the spectral structure of the flow by examining the time series of heading variation at each measuring point. Figure 9 shows the time series of heading variations from the four closest measuring points to the separation point along the reattachment streamline. (where more than one depth was measured the time series collected at the deepest near-bed position is shown). The heading time series move sequentially top to bottom, from upstream, near the separation point, to downstream. Because of the generally short time series (about 4-8 minutes each), which limits the confidence of the spectral resolution in the low frequency range, and the sparse coverage of the eddy, the discussion here is limited to general qualitative observations. An initial inspection of the time series in Figure 9 shows that those measuring locations near the separation point have more relatively high-frequency variability than those points further downstream. We look in more detail at these four measuring points downstream of the separation point (points 1,2,4, and 5 on Figure 8) to gain some insight into the evolution of the frequency structure of the flow, ignoring those points downstream of position 5 which may be complicated by the large topographic perturbation at measuring point 6 (see Figure 9). In general, the frequency shifts from relatively high-frequency low amplitude variability near the separation point to low-frequency high amplitude variability downstream from the separation point. Spectral analysis of these four time series (Figure 10) show that the peak in spectral energy in all cases is in the low frequency range ($\sim .02$ Hz); however, in the first time series there is a high frequency peak ($\sim .05 - .06$ Hz). No

direct measurement of vortex shedding was made in the field, but visual observations showed vortex shedding in the range of .05 - .1 Hz. In the time series recorded downstream of the first, the spectra becomes more broad and diffuse, in general agreement with flume observations made along the reattachment streamline of both a negative step (Eaton and Johnson, 1980) and a separation eddy (Rubin and McDonald, 1995; Nelson et al., 1995).

Sediment-trapping mechanisms

Previous studies of lateral separation eddies have identified three essential mechanisms producing transport of sediment across the reattachment streamline; 1) turbulent diffusion, 2) secondary flow, and 3) unsteadiness of the reattaching shear layer. In the past, turbulent diffusion of sediment from the relatively high-concentration main channel into the relatively low-concentration recirculation zone has been called upon to explain and model the trapping of sediment in the recirculation zone (Andrews, 1991). While this process clearly plays an important role, it underpredicts the trapping of sediment in simple flume experiments that identify secondary flow as an important sediment trapping mechanism (Nelson et al., 1994).

As previously noted, time-averaged flow fields that incorporate secondary flow appear to give good predictions of the evolution of eddy bar deposits generated in flume experiments. However, there is considerable low-frequency variation of both flow magnitude and direction in lateral separation eddies reflecting the inherently unsteady nature of flow in these features. Laboratory measurements show that the pattern of

secondary flow evolves downstream, with the strongest flow into the eddy order 1-3 expansion widths downstream of the separation point, after which the secondary flow loses strength (Nelson et al., 1995). This downstream pattern of relatively weak - strong - weak secondary flow reflects the evolution and tilting of the vortices axes of rotation as they are advected downstream and the eventual break up of the vortices as their energy dissipates. In addition to this time-averaged phenomenon, there is temporal variability about the pattern of secondary flow, characterized by strong pulsations of flow both into and out of the eddy throughout the flow depth. Spectral analysis of laboratory velocity time series show that the frequency of these pulsations are well scaled by the Strouhal number ($S = n d / U_{\infty}$, where S is the Strouhal number, n is the frequency of vortex shedding, d is the channel expansion width and U_{∞} is the far-field velocity) indicating that they are produced by the passage of vortices generated in the free shear layer downstream of the separation point.

In addition to the variability of secondary flow there is also considerable variability of the flow field associated with the reattaching shear layer exhibited in both the large upstream-downstream flow reversals about the mean reattachment point (Rubin et al., 1990 and Rubin and McDonald, 1995) and the change in position of the mean reattachment point with variations in discharge (Schmidt and Graf, 1990; Schmidt 1990, Schmidt et al., 1992). Either of these effects produce changes in the position between upstream and downstream flow or, in other words, between transport of sediment into or out of the eddy. The relative importance of these effects in trapping sediment remains unknown.

While not necessarily affecting the rate of sediment trapping, the size of the sediment trapping region dictated by the relation between discharge and reattachment length clearly modifies the quantity of sediment trapped from the main channel over the duration of some given sediment-transporting event. The effect of upstream-downstream flow fluctuations on sediment trapping is complicated and depends on whether or not there is any correlation between the magnitude of the upstream velocity with the change in the instantaneous position of the reattachment point. For example, if the magnitude of upstream velocity was greater when the instantaneous reattachment point was shifting downstream then sediment trapping would be enhanced. The latter relationship remains largely unexplored and may be an important contribution to sediment trapping.

In contrast to the geometry of the simple flat-bedded laboratory setting, the lateral separation eddies in the Grand Canyon are filled with large sediment deposits with steep slopes on the channel margin of the eddy deposit, at times approaching the angle of repose (Figure 6). In this region, there are significant differences in the characteristics of the flow situation that distinguish the natural setting from the simplified laboratory one. Based on measurements of both the velocity field and topography, three additional mechanisms that can be identified, each of which could potentially modify sediment trapping relative to the effects acting in simple flat-bedded eddies: (1) gravitational effects on sediment fluxes, (2) modification of mean secondary flows by the direct effects of steep lateral slopes, and (3) modification of secondary flows by anisotropy in the turbulence field. In contrast to the previously described mechanisms that act (in simple eddies) to enhance sediment flux into the eddy, these additional effects, described in the following paragraphs, act to possibly

inhibit sediment trapping and may be indicative of stable eddy deposits over the range of discharges during the field experiment.

On the channel-margin slopes of the eddy, gravitational forces can produce a significant correction to sediment fluxes. Whether the flow is downstream or upstream along the margin of the eddy deposit, gravity will produce a component of the bedload transport vector into the main channel (Parker, 1978). If the flow is either into or out of the eddy, gravity will act to inhibit bedload transport into or enhance bedload transport out of the eddy, respectively. Thus, we expect that gravitational correction to the sediment transport field can play an important role in the determination of equilibrium eddy-deposit morphology.

In contrast to the preceding mechanism, which is a direct response of the sediment transport field to the topography, the following arises from the interaction of the flow field with the topography. Measurements at Site 1 indicate that the form of secondary flow generated in the simple flat-bedded lateral recirculation zones may not be present in these eddies at all locations along the reattachment streamline. For example, at measuring positions 7 and 8 at Site 1 (Figure 7), the rose diagrams show there is both a distinct bimodal distribution of flow direction and a tendency for outward flow direction at depth. While the flow directions as represented in the rose diagrams do not indicate secondary flow (they contain only information about flow direction, not magnitude), the large component of flow direction away from the eddy into the main channel is contrary to what one would expect based on measurements in the flat-bedded case. The bimodality of the flow directions may be an indication of "flapping" or very low-frequency lateral

oscillations of the reattachment zone (Driver et al., 1987). In the case where the reattachment streamline is adjacent to a steep lateral slope, interactions of the flow with the topography will become important. For example, if movement of the reattachment streamline toward the eddy produces a situation where this streamline is oriented obliquely to the steep lateral slope, non-hydrostatic effects will produce changes in the vertical structure of the flow, the curvature of the reattachment streamline may be altered, and the vortex dynamics along the free shear layer will change. Each of these topographic effects can decrease or even reverse the sign of the secondary flow produced by the interaction of the free shear layer with the bottom boundary layer (or, equivalently, by streamline curvature) in the flat-bedded case.

In addition to modifications of the secondary flows by the direct effects of the steep lateral slopes found along well-developed eddy deposits, these flows may be indirectly altered through changes in the turbulence field. Along the reattachment streamline at Site 1 there exists a consistent high-velocity core at depth, and vertical profiles of mean secondary flow display a complicated pattern of secondary flow that, as noted above, sometimes displays outward flow near the bed into the main channel, especially in regions of steep lateral slopes. Because the quality of the secondary profiles are relatively poor, as previously discussed, they should be interpreted with caution. Nevertheless, these results are generally consistent with flume studies designed to look at flow and sediment transport interactions near a steep lateral slope between a main channel and flood plain (Knight and Demetriou, 1983; Knight and Hamed, 1984; Panagiotis et al. 1985; and Tominaga and Nezu, 1991). In these flume studies, a high velocity core is present and may be attributed

to the exchange of high and low momentum fluid between the relatively deep and shallow portions of the channel, respectively. These flume studies also show a complicated pattern of secondary flow generated from anisotropy in the turbulence field that, depending on the geometry of the lateral slope, may include outward flow into the main channel at depth. Flow in lateral recirculation zones near the channel margin break in slope of the eddy deposit is not perfectly analogous to flow interactions between a main channel and flood plain (e.g. there may be upstream flow along the channel margin of the eddy deposit at some discharges, as shown in Figure 8). However, there may be alterations in the patterns of secondary flow resulting from anisotropy of the turbulence field that are specifically driven by the steep lateral slopes.

The pattern of secondary flow found in the simple flume experiments should be characteristic of empty eddies. As the eddy fills with sediment and the geometry of the recirculation zone changes there should be a commensurate change in the pattern of flow. Our measurements (based on the distinct outward components of flow direction at depth, displayed in the rose diagrams at site 1 for measuring positions 7 and 8), which were made at flows significantly lower than those associated with formation of the eddy deposits, appear to indicate that in the deep pool adjacent to the eddy where the channel margins are relatively steep this change is manifested as a change in the pattern of flow direction to include outward flow at depth and inward flow near the surface. This evolution in the flow pattern may play an important role in the size and stability of the reattachment bar by limiting the flux of sediment into the eddy. Clearly, a more complete mapping of the flow field, particularly along and across the channel margin of the eddy deposit, is required to

better understand the interaction of topography and flow in natural eddies. The system is clearly complicated by relatively low-frequency energy associated with vortices generated in the free-shear layer and variations in the geometry of the reattachment zone and the position of the reattachment point. A complete understanding of the mechanisms of sediment trapping in these systems requires a better understanding of their inherent unsteady nature.

Conclusions

1. Mechanical current meters are susceptible to damping and clogging from suspended organic material which can wrap around an impeller axle or block the current meter duct. In rivers with significant amounts of suspended organic material non-mechanical current meters such as acoustic doppler velocimeters may provide better and longer velocity time series records.
2. Vertically-averaged velocity profiles show a rotary pattern of flow in lateral separation eddies generally consistent with patterns constructed from observation of surface tracers. Interaction of the flow field with the topography in lateral recirculation zones appears to have a significant affect on the vertical structure of the flow field not observed in previous flat-bedded flume studies. Non-hydrostatic effects, changes in streamline curvature, vortex dynamics and anisotropy of the turbulence field, all of which may result from this latter interaction, should be considered in a more detailed study of the flow field in natural sediment-filled lateral recirculation zones
3. Flow in lateral recirculation zones is inherently unsteady. Both the local and spatial pattern of temporal variations in flow direction and magnitude is complex and may

result from any of the following related effects: (1) generation and downstream evolution of vortices generated in the free shear layer along the reattachment streamline, (2) upstream-downstream fluctuations of both the instantaneous and time-averaged reattachment point, and (3) lateral fluctuations of the reattachment streamline. Our measurements suggest each of these three effects is important, and computational models of flow and bed evolution must incorporate these effects either directly or parametrically.

References

- Driver, D.M., H.L. Seegmiller, J. Marvin, Time-dependent behavior of a reattaching shear layer, *AIAA J.*, 19, 1093-1100, 1987.
- Eaton, J.K., and J. P. Johnson, Turbulent flow reattachment: An experimental study of the flow and structure behind a backward facing step, *Dep. of Mech. Eng. Rep. MD-39*, Stanford Univ., Stanford Calif., 1980
- Howard, A. D., and R. Dolan, Geomorphology of the Colorado River, *J. Geol.*, 89, 269-298, 1981.
- Kearsley, L. H., J. C. Schmidt, and K. D. Warren, Effects of Glen Canyon Dam on Colorado River sand deposits used as campsites in Grand Canyon National Park, USA, *Regulated Rivers*, 9, 137-149, 1994.
- Kieffer, S. W., The 1983 hydraulic jump at Crystal Rapid: Implications for river-running and geomorphic evolution in the Grand Canyon, *J. Geol.*, 93, 385-406, 1985.

- Knight, D.W., and J. D. Demetriou, Flood plain and main flow interaction, *Journal Hydraulic Engineering*, ASCE, 110, 1073-1092, 1984
- Knight, D.W. and M. E. Hamed, Boundary shear in symmetrical open channels, *Journal Hydraulic Engineering*, ASCE, 110, 1412-1430, 1984
- Leopold, L. B., The rapids and the pools of Grand Canyon, *U.S. Geol. Surv. Prof. Pap.*, 669-D, 1964.
- Miller, A. J., Debris-fan constrictions and flood hydraulics in river canyons: some implications from two-dimensional flow modeling, *Earth Surf. Processes Ldfms.*, 20, 1995.
- McDonald, R.R. and J. M. Nelson, USGS OPEN FILE REPORT (in prep.)
- Nelson, J. M., Experimental and theoretical investigation of lateral separation eddies, *Eos Trans. AGU*, 72, 218-219, 1991.
- Nelson, J. M., R. R. McDonald and D. M. Rubin., Computational prediction of flow and sediment transport patterns in lateral separation eddies, *Eos Trans. AGU*, 75, 268, 1994.
- Nelson, J.M., R. I. Shreve, S.R. McLean, and T. G. Drake, Role of near-bed turbulence structure in bed load transport and bed form mechanics, *Water Resour. Res.*, 31, 2071-2086, 1995.
- Nelson, J. M., R. R. McDonald and D. M. Rubin., Flow and sediment transport in lateral separation eddies, (submitted), 1995.
- Panagiotis, P., R. Townsend., and T. Stravros, Structure of turbulence in compound channel flows, *Journal Hydraulic Engineering*, ASCE, 111, 1246-1261, 1985.

- Parker, G., Self-formed equilibrium banks and mobile bed. Part 1. The sand-silt river, *J. Fluid Mech.*, 89, 109-125, 1978.
- Rubin, D. M., J. C. Schmidt, and J. N. Moore, Origin, Structure and evolution of a reattachment bar, Colorado River, Grand Canyon, Arizona, *J. Sediment. Petrol.*, 60, 982-991, 1990.
- Rubin, D. M. and R. R. McDonald, Nonperiodic eddy pulsations, In press (*Water Resources Research*) 1995.
- Schmidt, J. C., Recirculating flow and sedimentation in the Colorado River in Grand Canyon, Arizona, *J. Geol.*, 98, 709-724, 1990.
- Schmidt, J. C. and J. B. Graf, Aggradation and degradation of alluvial sand deposits, 1965 to 1986, Colorado River, Grand Canyon National Park, Arizona, *U.S. Geol. Surv. Prof. Pap.*, 1493, 1990.
- Schmidt, J. C., D. M. Rubin., and H. Ikeda, Flume simulation of recirculating flow and sedimentation, *Water Resour. Res.*, 29, 2925-2939, 1992.
- Schmidt, J.C. and D. M. Rubin, Regulated streamflow, fine-grained deposits, and effective discharge in canyons with abundant debris fans, In: Natural and Anthropogenic Influences in Fluvial Geomorphology, edited by J.E. Costa, et al. *Geophysical Monograph 89*, AGU, 1995.
- Simpson, R.L., Turbulent boundary-layer separation, *Ann. Rev. Fluid Mech.*, 21, 205-234, 1989.

Smith, J.D., Measurement of turbulence in ocean boundary layers, paper presented at Working Conference on Current Measurement, Office Ocean Eng., Natl. Oceanic and Atmos. Admin., Univ. of Del. Newark, Del., Jan 11-13, 1978.

Smith, W.H.F. and P. Wessel, Gridding with continuous curvature splines in tension, *Geophysics*, 55, 293-305, 1990

Tominaga, A. and I. Nezu, Turbulent structure in compound open-channel flows, *Journal of Hydraulic Engineering*, ASCE, 117, 21-41, 1991.

Figure Captions

- Figure 1: A) General sketch of lateral separation zone flow features and B) sedimentary features and channel morphology. Adapted from Schmidt and Graf (1990).
- Figure 2: Aerial Photographs of the three study sites taken approximately four months before our field study. A) Eminence Break Eddy, B) Carbon Creek Eddy, and C) Mile 122 Eddy.
- Figure 3: A) Discharge History at Lee's Ferry River Mile 0, for the month of September, 1993. B) A close up showing the steady flow at high discharge measured at all three sites and the near steady low flow measured at site 3.
- Figure 4: Complete current meter profiling system. Note the four sets of current meter triplets, lead weights at the bottom, large fin, and the signal junction box just above the fin.
- Figure 5: A persistent problem in our data collection was contamination from suspended organic matter leading to clogging and fouling of the current meters. Here we show a sample of both good (A) and contaminated data (B), where in the latter case the first third of the data is damped, the second third is good, and the last third is completely clogged.
- Figure 6: Topographic cross-sections at measuring position 2 and 11, (A) and (B) respectively, at Site 1 and measuring position 7 and 27, (C) and (D) respectively at Site 2 (See Figures 7 and 8 below for relative position of each measuring point). Each cross-section intersects the labeled measuring position and is perpendicular to the trend of the thalweg at each site. The vertical

component is exaggerated two times. At both sites the eddy is located on the right side of the cross section.

Figure 7: Topographic and mean vertically averaged velocity vector maps of Eminence Break Eddy. The map in the lower right is a topographic map of the reach at Eminence Break Eddy; the contour interval is 1 meter and the flow is from top to bottom. The red dots are the location of each measuring position. The topographic map at the upper right is a close up of the region in which flow was measured. The arrows are the mean vertically averaged vectors with the tails centered on the measuring position. The variation in flow direction at each site as recorded in the compass is plotted as rose diagrams to the left. The red rose diagrams represent the near surface location at each position and the position of each site relative to each other is preserved and simply scaled up to accommodate all the positions. Positions that measured more than one depth contain multiple rose diagrams with yellow-green-blue colors in descending order of relative depth. The distance separating rose diagrams at each point are not necessarily scaled but in general divide the total depth evenly.

Figure 8: Topographic map of mean vertically averaged velocity vectors for Mile 122 Eddy at both high and low flow. The reach scale topographic map is at the lower left. The colored circles represent the measuring positions; yellow at low discharge and red at high discharge. The two smaller topographic maps at the lower right are close-up maps of both low and high discharge and the

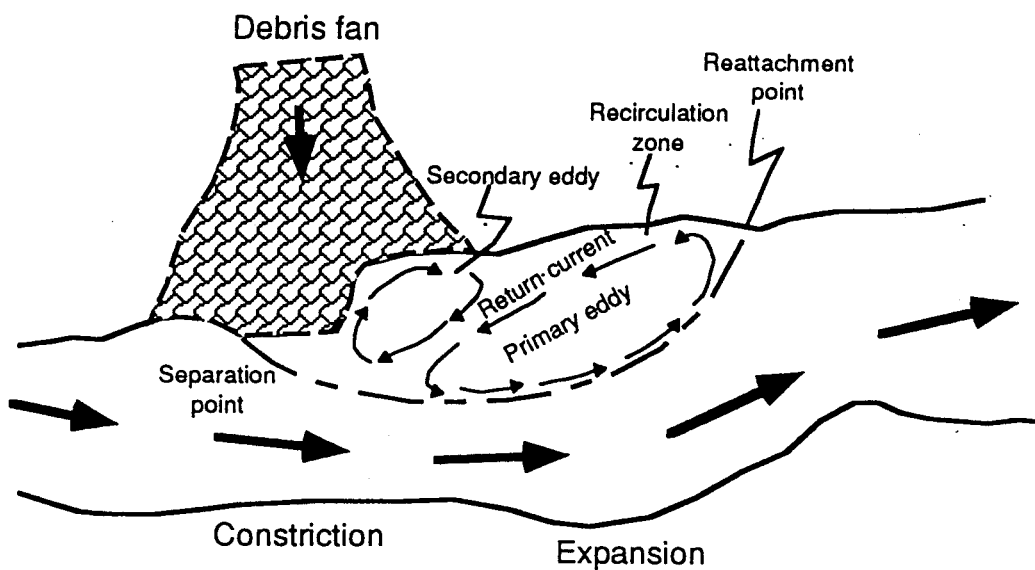
vectors have the same format as Figure 6. The variations in flow direction are plotted as rose diagrams. The near-surface measuring locations are colored yellow for high discharge and red for low discharge. At those sites where more than one depth was measured, rose diagrams are appended with green and blue colors in order of descending depths. The distance between rose diagrams with more than one depth measured is arbitrary and not necessarily scaled to the relative depth at each position.

Figure 9: Time series of heading variations at Site 3, low-discharge measuring positions 1,2,4 & 5. The variations of heading record the change in direction of the fin located on the current meter profiler. Because the fin responds to low-frequency fluctuations, it is ideal for looking at flow variations associated with the passage of large-scale eddy structures produced in the free shear layer just downstream from the separation point. The position of each time series is labeled near the top-center.

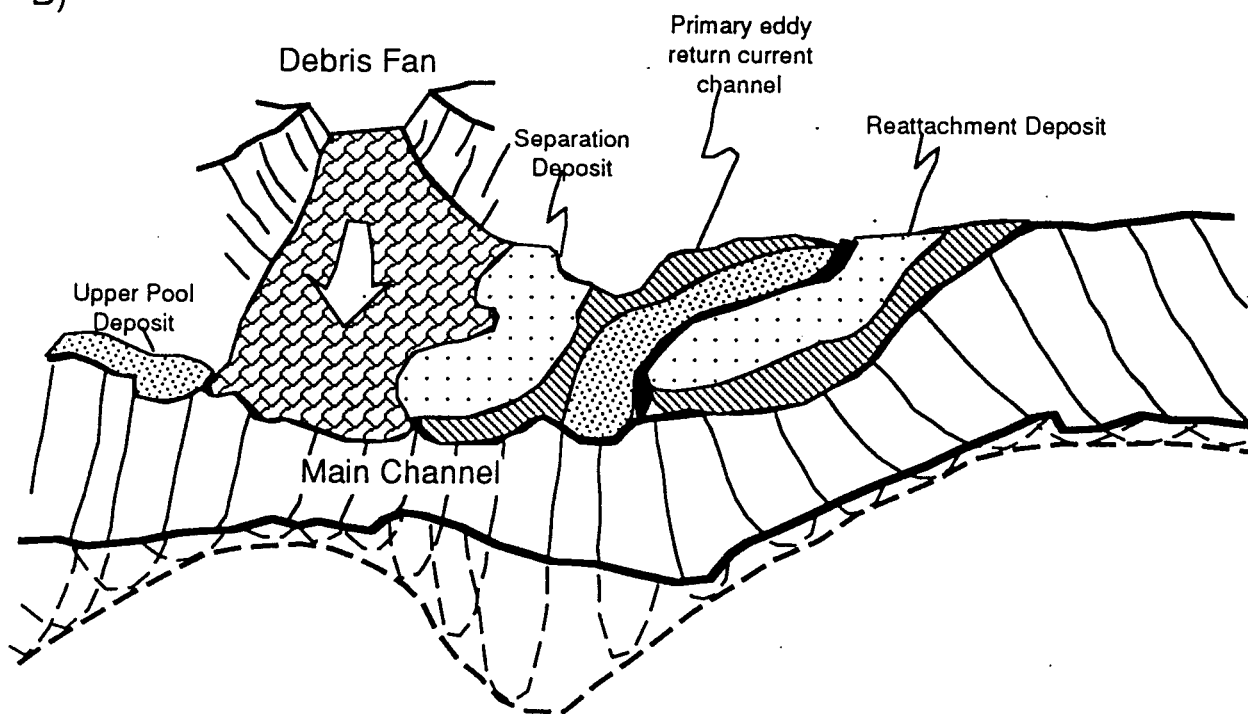
Figure 10: Power spectral density plots of heading variations from the first four heading time series of Figure 9. Each time series was broken into 2 segments of 2048 points each to calculate the power spectral density. Only the low-frequency range (up to 0.2 Hz) is shown. Note that moving in the downstream direction (Figure A-D) there is a general increase in the power of the low-frequency peak at ~ 0.02 Hz and a decrease in power of the higher frequency peak ~ 0.055 Hz. Additionally there is a general trend of power to switch from

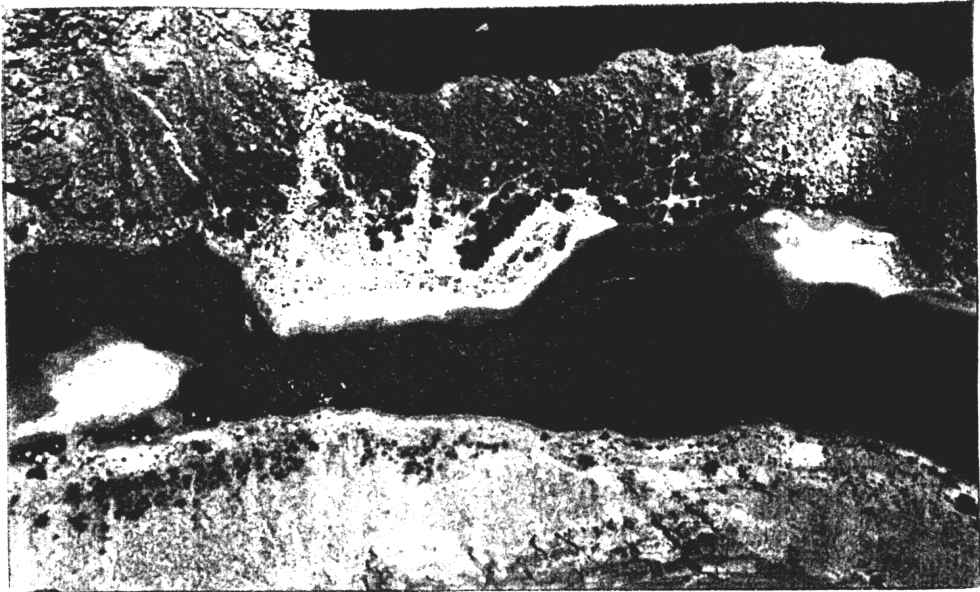
relatively high-frequencies associated with small amplitude variations to lower frequencies associated with large amplitude variations.

A)

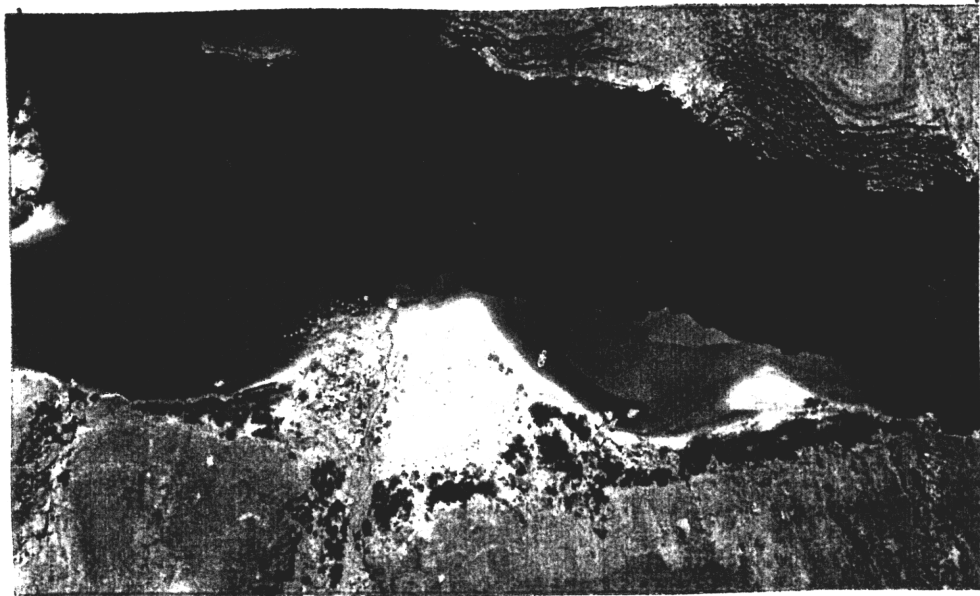


B)



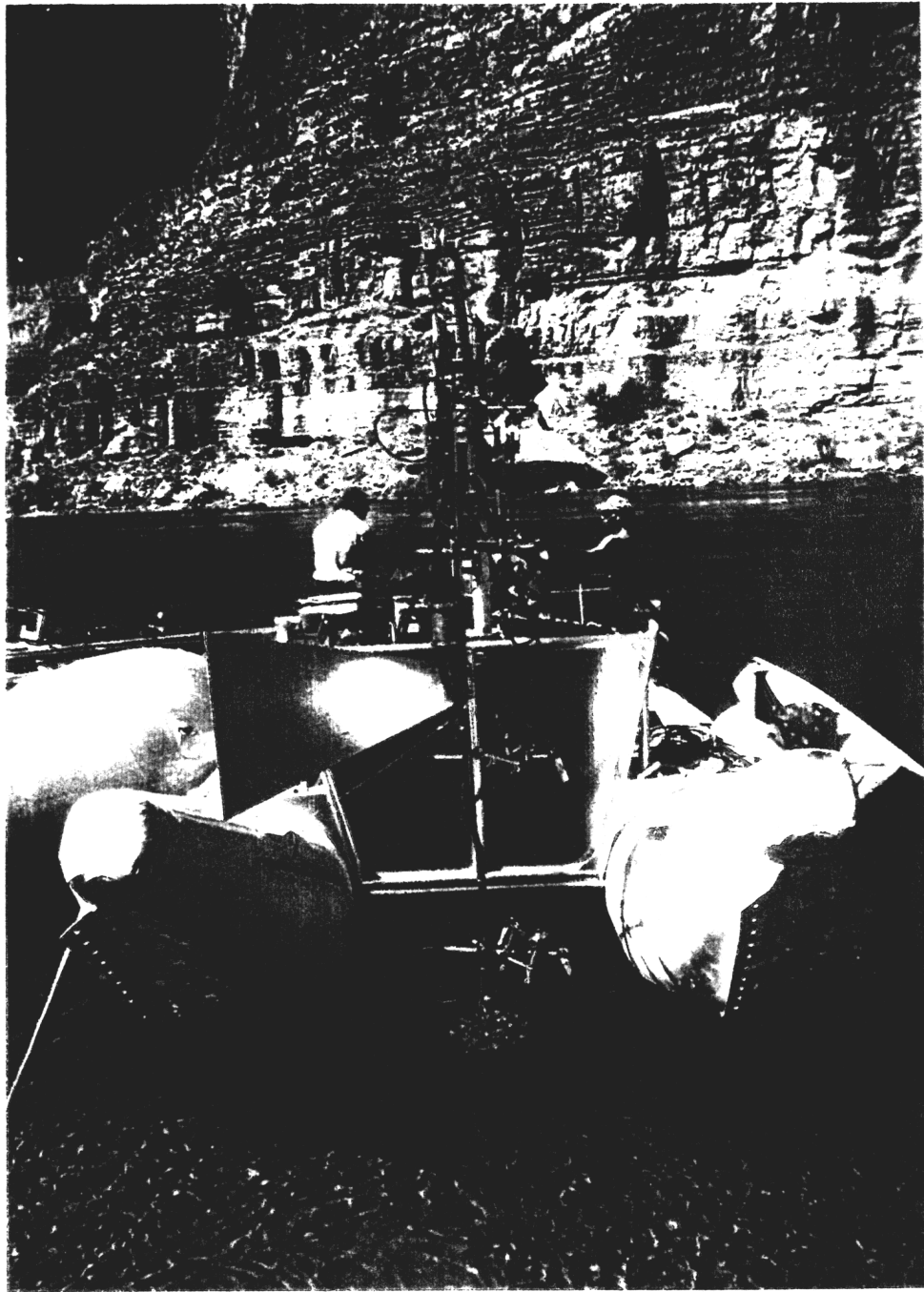


(A)

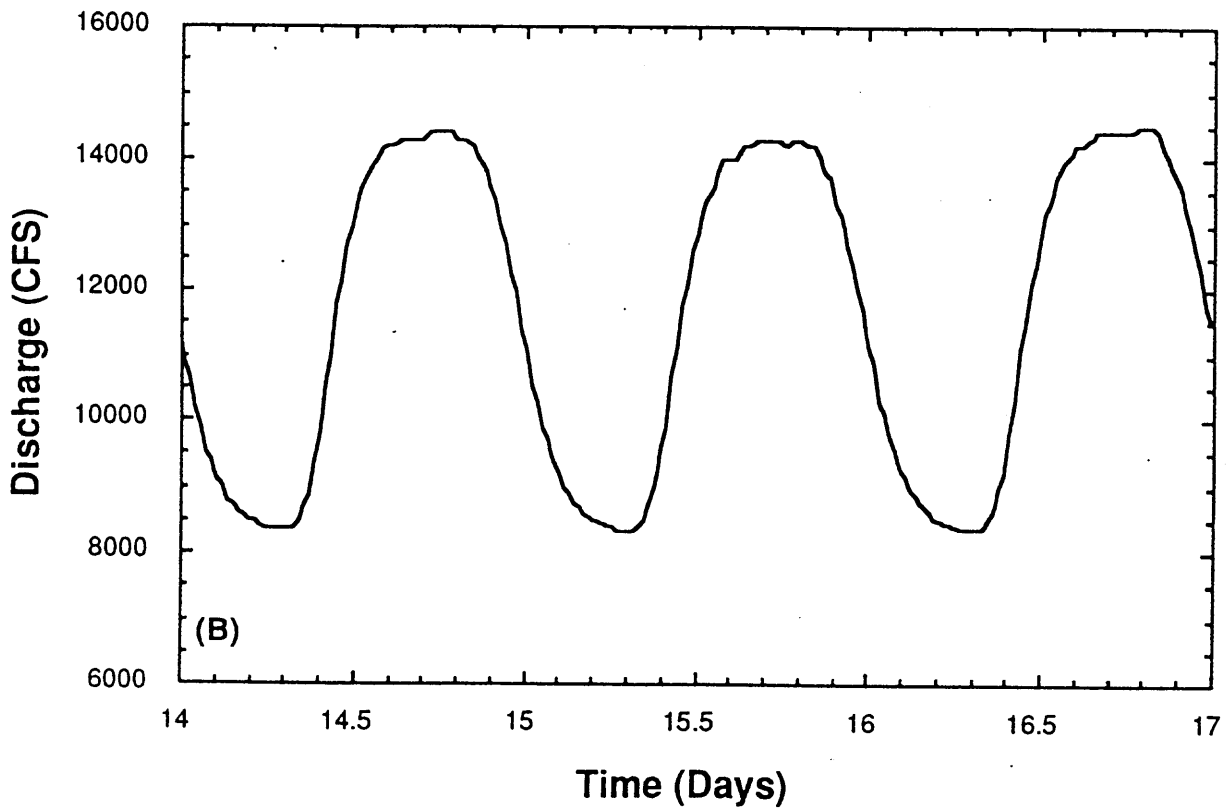
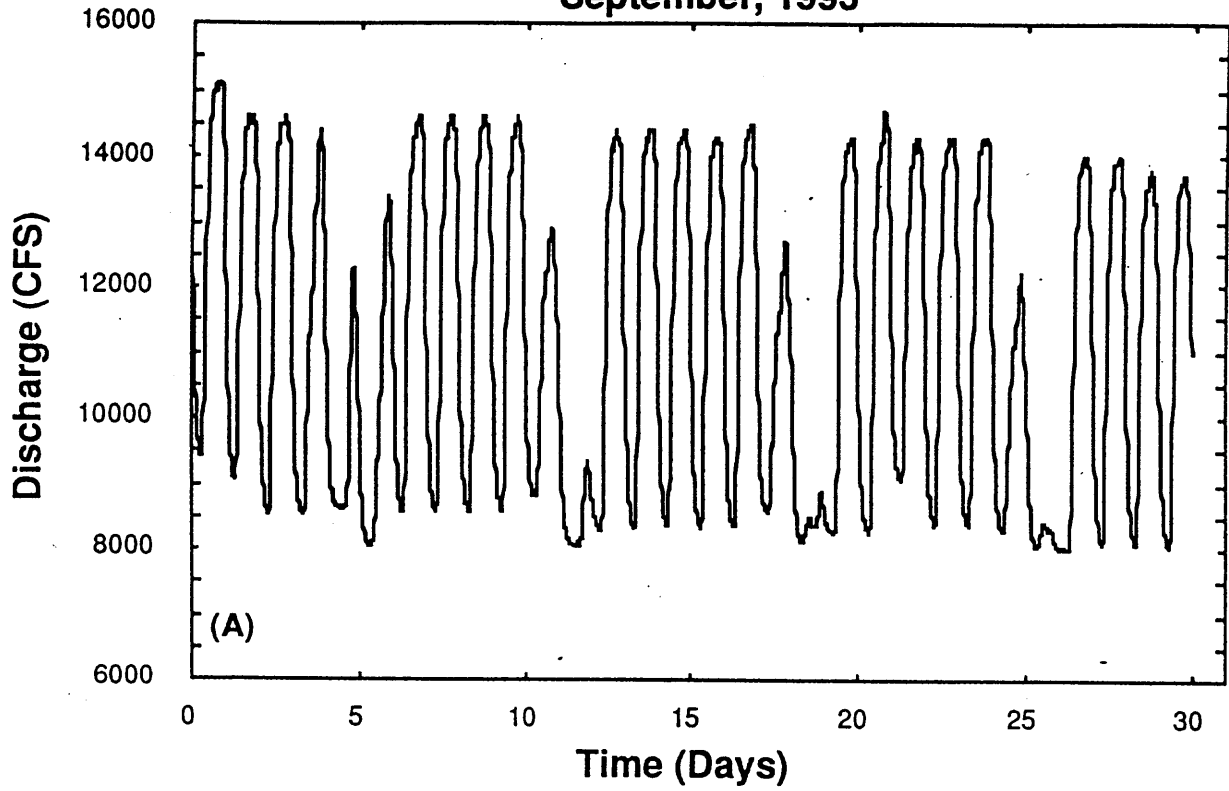


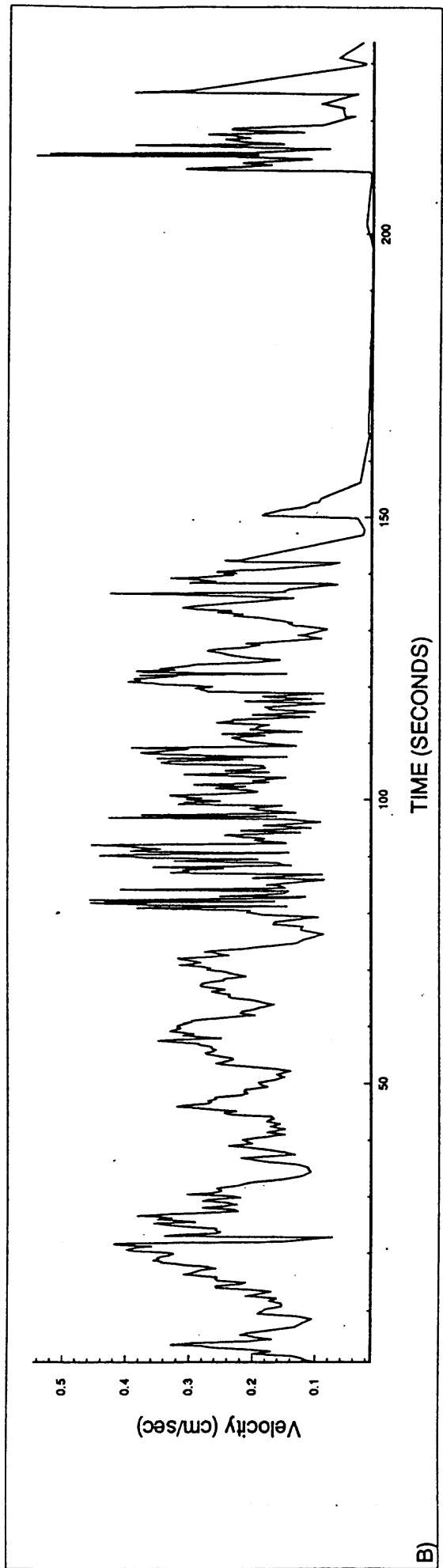
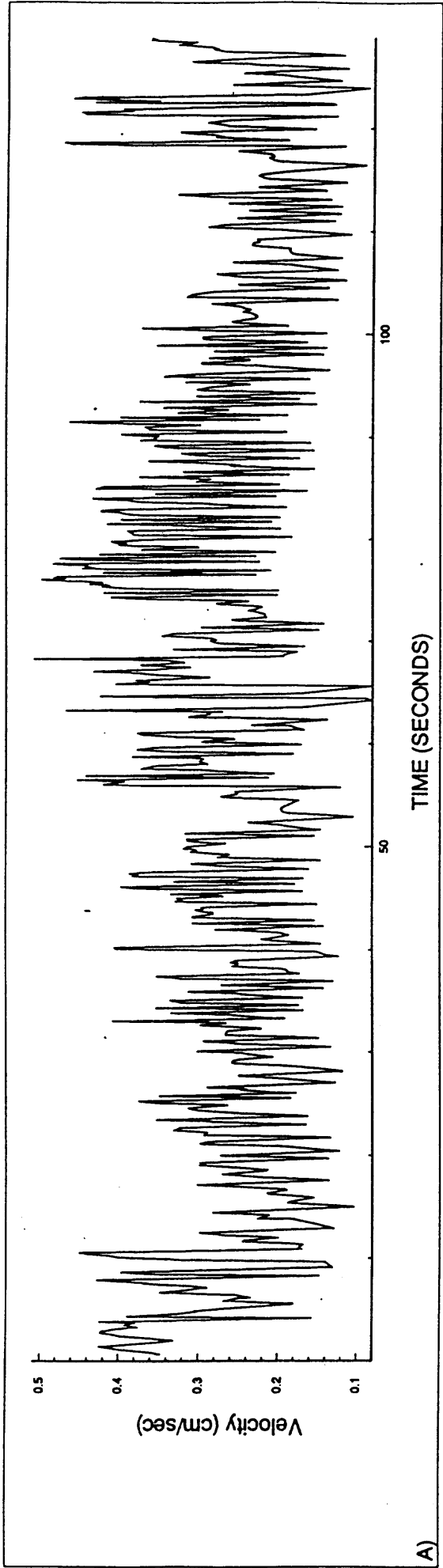
(B)

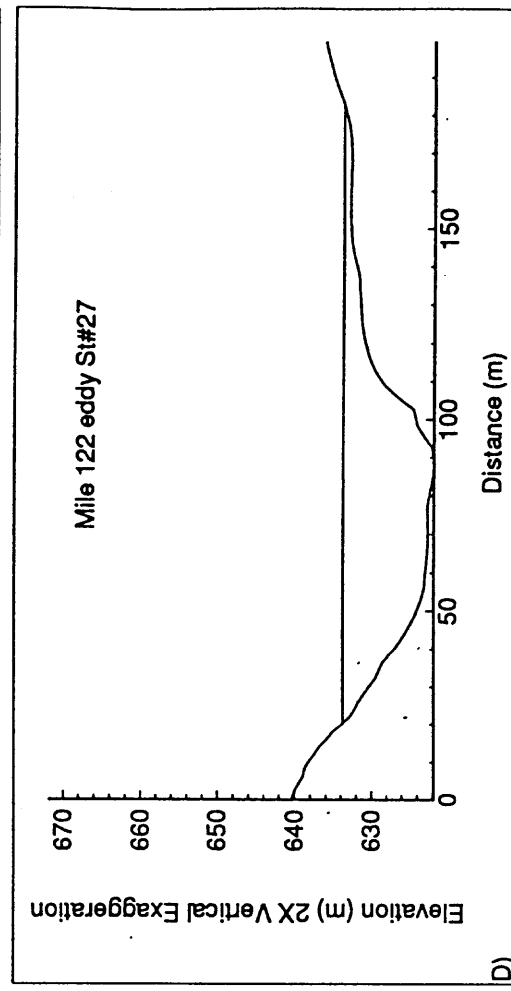
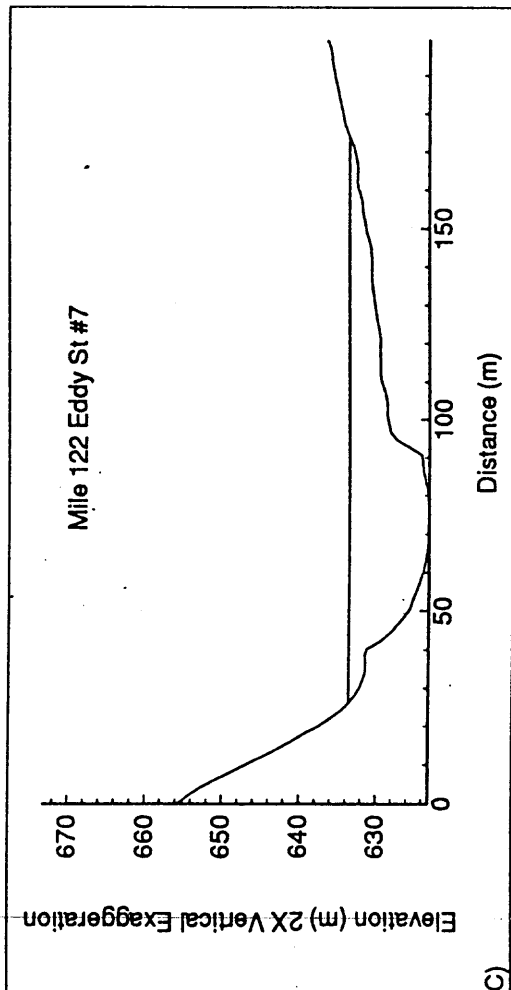
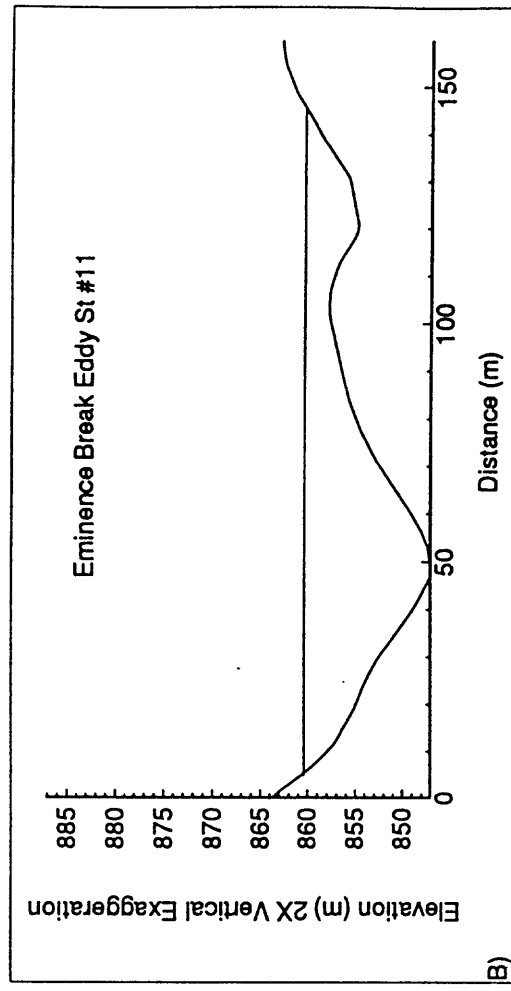
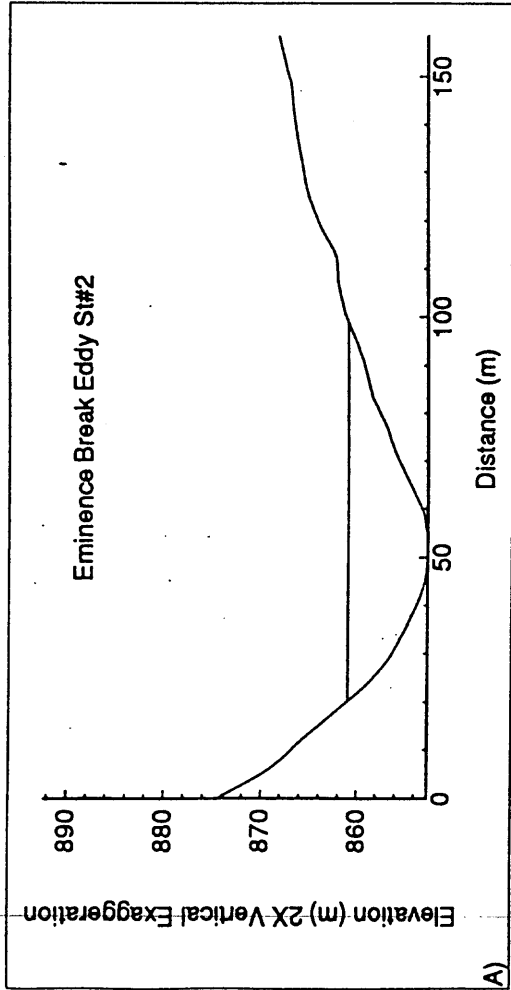




Discharge history at Lee's Ferry -River mile 0
September, 1993





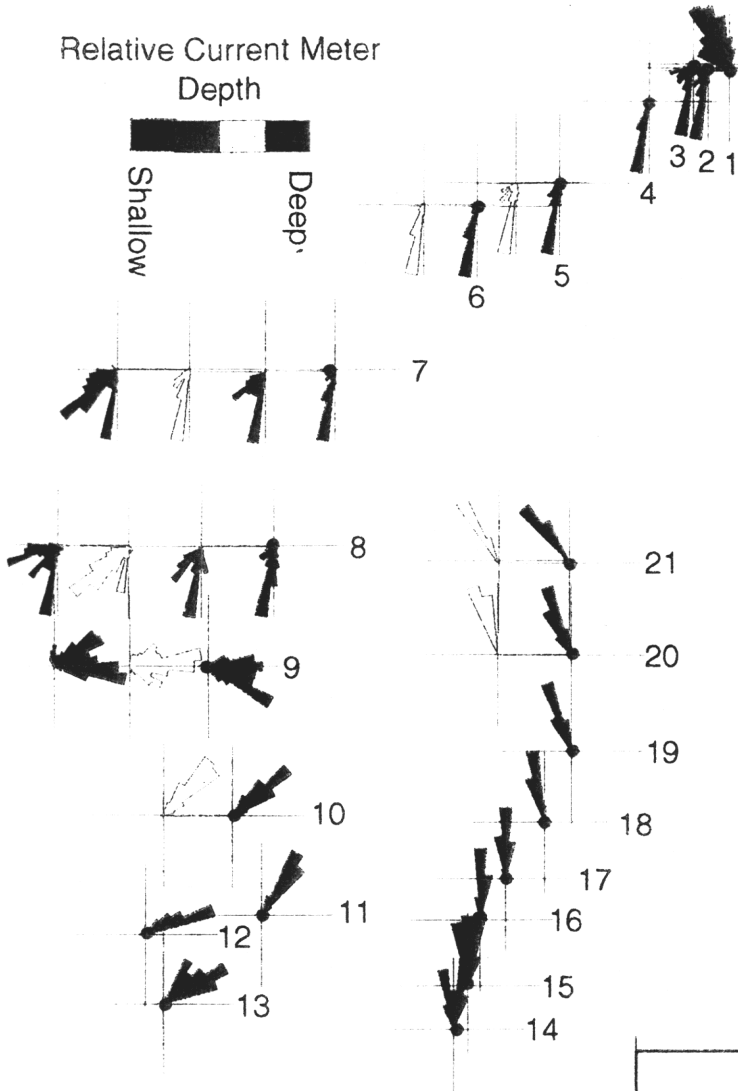


Relative Current Meter
Depth



Shallow

Deep



597500

597400

597300

219300

219400

NORTHING (m)

EASTING (m)



865

860

855

850

845

NORTHING (m)

597500

597400

597300

597200

219100

219200

219300

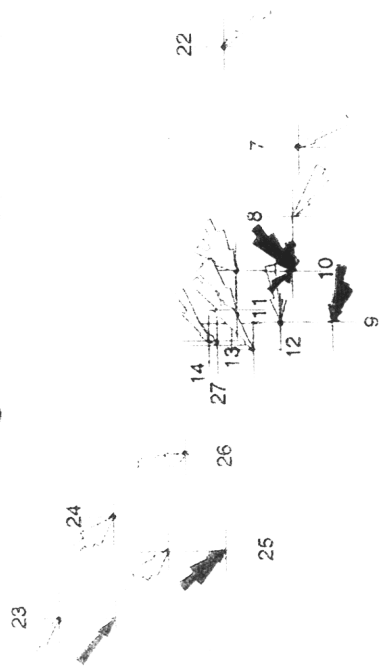
219400

219500

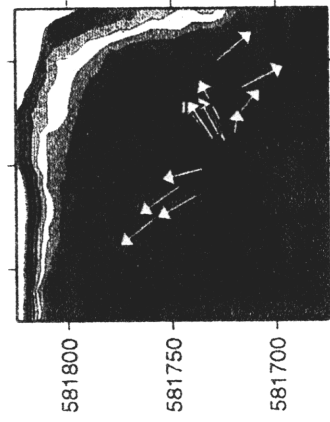
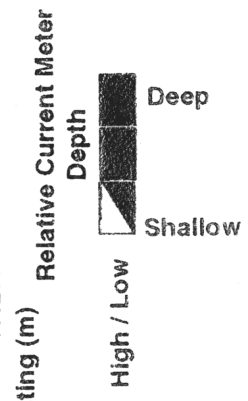
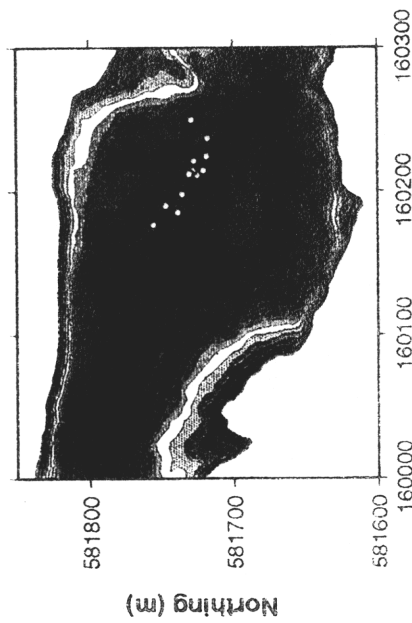
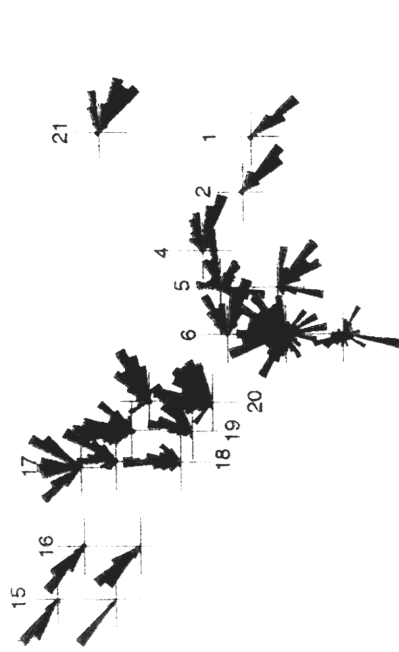
EASTING (m)

Mile 122 Eddy

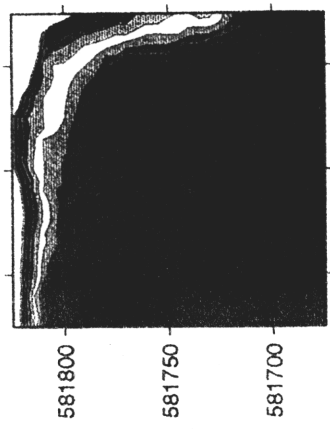
High Discharge



Low Discharge



High Discharge.



Low Discharge

